Diffusion–convection impedance for a micro-band electrode under microfluidic conditions

Claire Poujouly, Pedro Gonzalez-Losada, Rassen Boukraa, Martina Freisa, Jérémy Le Gall, David Bouville, Claude Deslouis, Jean Gamby

Electrochemistry Communications 137 (2022) 107262

Contents lists available at ScienceDirect

Electrochemistry Communications

journal homepage: www.elsevier.com/locate/elecom

Short Communication

Diffusion–convection impedance for a micro-band electrode under microfluidic conditions

Claire Poujouly [a], Pedro Gonzalez-Losada [a], Rassen Boukraa [a], Martina Freisa [a], Jérémy Le Gall [a], David Bouville [a], Claude Deslouis [b], Jean Gamby [a,*]

[a] Université Paris-Saclay, CNRS, Centre de Nanosciences et de Nanotechnologies, 91120 Palaiseau, France
[b] Sorbonne Universités, UPMC Univ Paris 06, CNRS, Laboratoire Interfaces et Systèmes Electrochimiques, 4 place Jussieu, F-75005 Paris, France

ARTICLE INFO

Keywords:
Channel-electrode
Microfluidics
Impedance
Diffusion–convection
Reduced frequency

ABSTRACT

Diffusion–convection impedance for a micro-band electrode placed in a Poiseuille flow was studied experimentally under microfluidic conditions. Electrochemical impedance spectroscopy (EIS) experiments performed with a fast electrochemical system show perfect agreement with a previously published quantitative analytical expression in the low frequency domain.

1. Introduction

The use of a band microelectrode in a microfluidic channel, denoted a 'channel-microelectrode', offers two main advantages. First, a steady-state current response is reached rapidly (~1 ms) due to a diffusion layer which is thinner than the hydrodynamic boundary layer. Second, it is an efficient method of drastically reducing the sample volume, improving the system dynamics, and increasing the analytical performance of the sensor [1,2,3,4]. According to previous reports using hydrodynamic voltammetry, the higher the flow rate, the thinner the diffusion layer [5,6,7,8]. A higher current density is moreover expected at the electrode when the flow rate is increased. It is however mandatory for the flow rate to have a value small enough to remain within the limits of the pre-established model. This relies on the dimensionless Péclet number ($P_e = R_e \times S_c$, where R_e is the Reynolds number and S_c the Schmidt number) which quantifies the importance of the convective flux with respect to the diffusive flux [9]. For $P_e \gg 1$ close to the electrode, the convective effect dominates over diffusive transport, so that the flow rate is higher and the formation of a small diffusion layer is ensured.

The diffusion–convection impedance is one of the elements included in the overall impedance measured for an electrochemical system by electrochemical impedance spectroscopy (EIS) and can be simulated using a Randles equivalent circuit [10].

The case of pure diffusion conditions for microelectrodes of different shapes has been treated by Fleishman et al. [11] and also confirmed for a microelectrode tip without flow [12] at the low frequency limit. This case would be relevant only for very low flow rates. At higher flow rates this expression is obviously inadequate whether the flow is open or in a microfluidic system.

A first treatment of diffusion–convection impedance for a band electrode was first proposed by Compton and Sealy [13], then experimentally applied in [14] for a channel electrode, with reasonable agreement. Later on, Deslouis et al. [15,16] calculated the diffusion convection impedance for both circular and rectangular microelectrodes in open systems using a numerical analysis technique: their approach pointed out that even for a microelectrode there is a local impedance response depending on the local distance from the leading edge with its own characteristic frequency and thus requiring integration over the whole microelectrode. Good agreement between experiment and theory was obtained for circular microelectrodes in a pipe flow with either laminar or turbulent flows [15]. In 1995, Compton and Winkler [17] examined the relative roles of axial diffusion and convective diffusion for microband electrodes in a microchannel on varying the electrode width or flow rate or both.

In recent years, analytical expressions of the diffusion–convection impedance in microfluidics using EIS have been used to study channel-electrode architecture under various flow rates [18,19,20,21,22,23].

In the present work, an experimental comparison with the quantitative theory proposed in [15,16] was carried out for microband electrodes in a rectangular microchannel of high aspect ratio. The applied

* Corresponding author.
E-mail address: jean.gamby@universite-paris-saclay.fr (J. Gamby).

https://doi.org/10.1016/j.elecom.2022.107262
Received 23 November 2021; Received in revised form 23 February 2022; Accepted 10 March 2022
Available online 12 March 2022

conditions were selected with a view to application as a DNA biosensor, in particular the choice of NaCl (0.5 M) as the medium, as in the previous work by Horny et al. [8,18]. These authors have also shown that the maximum fixed flow rate for a DNA biosensor application in the present geometry would be around 0.5 μL s^{-1}. Therefore the flow rates considered experimentally will fulfil this criterion, i.e. be below this value. Second, the restricted potential window for proper functioning of a DNA sensor imposes another constraint: a working potential close to the rest potential. Such conditions, where the relative importance of the diffusion impedance with respect to the charge transfer resistance is not as favourable as in studies performed at the half wave potential, require good accuracy in calculation of the former, as expected from the use of the expression given in [15,16].

2. Experimental

2.1. Chemicals and reagents

NaCl (purchased from Prolabo) and potassium hexacyanoferrate (III), $K_3[Fe(CN)_6]$ and potassium hexacyanoferrate (II) trihydrate, $K_4[Fe(CN)_6]\cdot 3H_2O$ (purchased from Prolabo) were used as supporting electrolyte and redox tracer, respectively. The influence of the sodium cation on the rate constant of the $Fe(CN)_6^{4-}/Fe(CN)_6^{3-}$ system was shown to be first order in that concentration range with k_0 values of a few 10^{-2} cm.s^{-1} [24].

All experiments were carried out in a temperature-controlled room (20 °C) with an air treatment station.

2.2. Microfluidic chip and microelectrode fabrication

As illustrated in Fig. 1(A-C), the microfluidic chip was composed of a gold working microelectrode (WE) (30 μm × 300 μm) and counter electrode (CE) (2 mm × 300 μm) patterned by photolithography and lift-off processes on a glass wafer. The chip was closed off with PDMS (ratio 1:10), patterned with a SU-8 mold and sealed by O_2 plasma bonding. The thickness of the gold deposit may be a source of perturbation with respect to the implicit hypothesis that the electrode surface is in the same plane as the insulating base support. The effect of setting the electrode in recessed or protruding positions with respect to the base support was considered by Alden and Compton [25] but only for pure diffusion conditions. The thickness of the gold film (200 nm) produced by the present fabrication process is small enough to bear any perturbation in either hydrodynamic or diffusion boundary layers.

The CE was set downstream of the WE and at a sufficient distance from it (about three times the electrode width) to avoid any perturbation on the diffusion layer in its wake.

The working electrode was set at 0.8 cm from the flow entrance. For a parallel Poiseuille flow, the entrance length L_e of the flow region beyond which the build-up of the parabolic velocity profile is fully established is $0.04 \times R_e \times h$. The highest R_e number is here equal to 0.67 so that $L_e \leq 27$ μm ≤ 8000 μm. For comparison, in a recent paper [26] the entrance length for a channel of similar aspect ratio was found to be equal to $0.4 \times d$ for $10^{-3} \leq Re \leq 10^2$ i.e. 120 μm, a distance which is much smaller than the position of the microband (0.8 cm) and thus ensures that the parabolic flow is well established at this point. The detailed protocol for WE gold microelectrode fabrication is as described in Horny et al. [18,23].

Considering the similar values of channel height and microelectrode width, one must consider the possibility of an edge effect when calculating the maximum local thickness of the diffusion layer, which is attained for $x = x_e$. This value corresponds to $3^{2/3}\,\Gamma(4/3)\,(Dx_e/\alpha)^{1/3}$, where D is the solute diffusion coefficient and α the wall velocity gradient. This thickness is higher for the lower α value (here 80 s^{-1}) which gives ~ 13 μm and is about 5 μm when α ~ 1600, values that are reasonably lower than the channel height (40 μm) and thus the diffusion layer is not constrained by the geometry of the opposite wall.

2.3. Instrumentation and measurements

The EIS measurements were carried out using a Biologic Potentiostat (SP 300) coupled with an ultralow current probe. The on-chip EIS measurements were performed with a two-electrode setup: a 30 μm wide

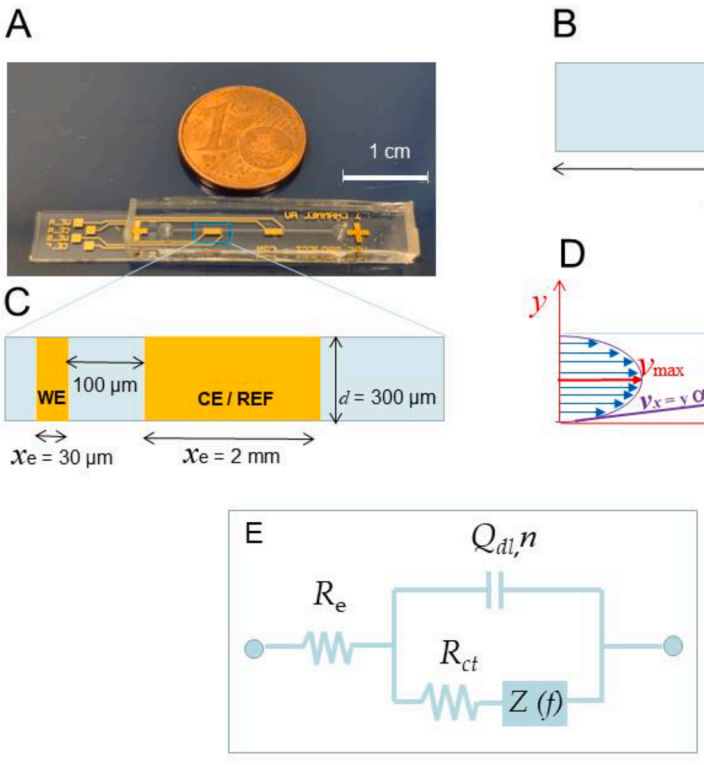

Fig. 1. (**A**) Global picture of the chip comprising two pairs of two-microelectrode networks. (**B**) Schematic cross-section view of the channel fluidic configuration where h and d represent the channel height and width, respectively. (**C**) Schematic top view of the microchannel electrode configuration where WE represents the working electrode (width, d = 300 μm, length x_e = 30 μm) and CE the counter electrode (d = 300 μm, x_e = 2 mm). (**D**) Schematic view of a 2-D channel electrode with developed Poiseuille flow (high aspect d/h ratio) with the steady-state diffusion–convection Eqs. (1)–(7). v_{max}, v_x, S and δ_{xe} are the maximum velocity of the developed parabolic flow, the linear approximation of the flow velocity, the wall velocity gradient, and the local diffusion layer thickness, respectively. (**E**) Electrical equivalent circuit proposed for simulation of the impedance plots.

Au microband working electrode and a 2 mm wide Au microband counter electrode (see Fig. 1C). Due to the high ratio of the CE area versus the WE area (~67) the CE was simultaneously used as a pseudo-reference electrode (REF) [18,23], at an equilibrium potential of 0 V with a 10 mV excitation signal between 1 MHz and 100 mHz. The experiments were performed in an equimolar solution of 3 mM $[Fe_{(III)}(CN)_6]^{3-}/[Fe_{(II)}(CN)_6]^{4-}$, with flow rates from 0.01 to 0.2 µL/s. The EIS experimental plots were simulated using the Simad software developed at LISE laboratory and based on a simplex procedure. A NEMESYS programmable syringe pump allowing a flow rate in the range from 0.01 µL.s^{-1} to 0.2 µL.s^{-1} was used to control the flow.

3. Results and discussion

The experimental EIS plots displayed as Nyquist and Bode representations (Fig. 2) were obtained in 3 mM ferri-ferrocyanide solution at the equilibrium potential with the lowest volumetric flow (0.01 µL s^{-1}). An appropriate modified Randles circuit was used to analyze the impedance data for each flow rate (Fig. 1D, E). The electrolyte resistance, R_e (related to electrolyte conductivity and depending on the channel microelectrode size), corresponds to the asymptotic limit in the HF domain of the real part (Z_R) in the Nyquist plot. The sum of R_e, the charge-transfer resistance R_{ct} (first semi-circle diameter) and the convection–diffusion resistance R_D (second semi-circle diameter) is the asymptotic limit in the LF domain of the real part (Z_R). A constant-phase element CPE (parameters Q_{dl} and n) was used in place of the double-layer capacitance (C_{dl}) to take account of the 2-D distribution ($n < 1$) of current and potential electrode [27,28,29]. This latter is arranged in parallel with R_{ct} in the HF domain.

The analytical equation for EIS fitting used in Fig. 2 and corresponding to the modified Randles circuit in Fig. 1(E) is expressed as follows [30]:.

$$Z(f) = R_e + \frac{(R_{ct} + Z_D(f))}{1 + (j2\pi f)^n Q_{dl}(R_{ct} + Z_D(f))} \quad (1)$$

Here the diffusion–convection impedance Z_D was calculated as in [16] and expressed as a function of a dimensionless frequency σ with two solutions valid in the LF and HF domains, respectively, matching around σ ~ 5.

LF solution:.

$$|Z_D(\sigma)| = |R_D(0)|\left(1 + 0.433\sigma^2 - 0.0084\sigma^4\right)^{-1/2} \quad (2)$$

$$\mathrm{Arg}(Z_D) = -\tan^{-1}\left\{0.5527\sigma\left(1 - 0.071\sigma^2 + 0.0023\sigma^4\right)\right\} \quad (3)$$

HF solution:.

$$|Z_D(\sigma)| = |R_D(0)|\frac{0.80755}{\sigma^{1/2}}\left(1 + \frac{0.1768}{\sigma^{3/2}}\right) \quad (4)$$

$$\mathrm{Arg}(Z_D) = -\tan^{-1}\left\{1 - \frac{0.3536}{\sigma^{3/2}}\right\} \quad (5)$$

$$\sigma = \omega\left(\frac{x_e^2}{D\alpha^2}\right)^{1/3} \quad \text{with} \quad \omega = 2\pi f \quad (6)$$

α is the wall velocity gradient, defined for a rectangular channel of high aspect ratio as:.

$$\alpha = \frac{6F_v}{h^2 d} \quad (7)$$

where F_v is the volumetric flow rate.

The fitting model built from the equations consists of five unknown parameters $R_e, R_{ct}, R_D(0), Q_{dl},$ and n. In the first step, it was checked that the LF solution defined by Eqs. (2) and (3) and that proposed in Refs. [13,17] give very close results, but as a HF solution was also necessary to determine the parameters R_e, R_{ct}, Q_{dl} and n (say around tens and hundreds of kilohertz), the regression of the theoretical impedance expression to the data based on a simplex strategy (using Simad software) was carried out using Eqs. (2)–(5) in this paper.

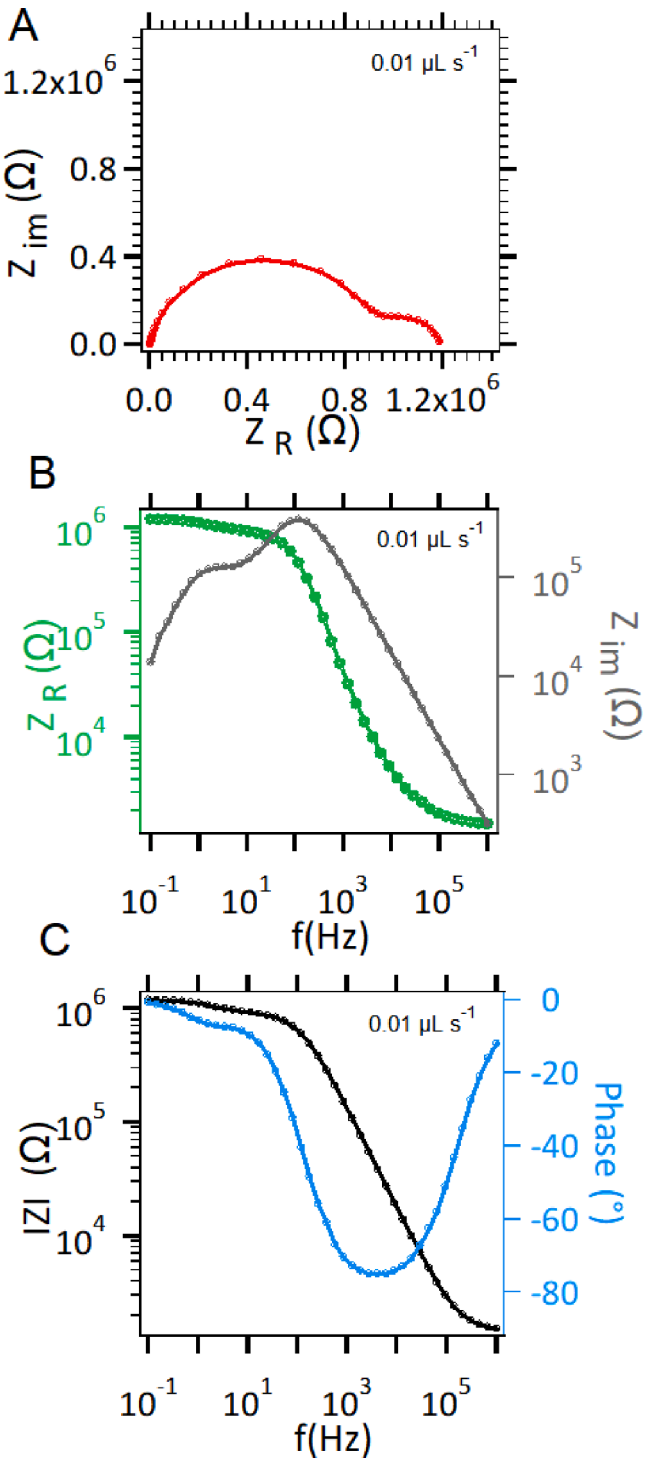

Fig. 2. (**A**) Nyquist representation of EIS data measured in a device filled at 0.01 µL s^{-1} with 3 mM $[Fe_{(III)}(CN)_6]^{3-}/[Fe_{(II)}(CN)_6]^{4-}$ in 0.5 M NaCl for frequencies from 1 MHz to 0.1 Hz with 10 mV AC signal excitation. (**B**) Bode representations of the EIS imaginary part (left axis) superimposed with the real part (right axis). (**C**) Bode representation of the EIS impedance phase (left axis) superimposed with the modulus part (right axis).

By analyzing the experimental plots and the pre-fitted ones with Eqs. (1)–(7), we fixed an initial value ~ 1450 Ω for R_e as $f \to +\infty$, at the intersection between the HF part of the curve and the x-axis. R_{ct} can also

be fixed as an initial guess by considering it to be the value of the first semi-circle diameter.

For $f \to 0$, equation (1) gives $Z_{eq}(0) = R_e + R_{ct} + R_D$, with $R_D = Z_D(0)$ then quite easily obtained from the second intersection between the curve and the x-axis. The five parameters mentioned above were determined by regression of the model (Eq. (1)) to the EIS data, starting from these initial approximate values and for different wall velocity gradients, α. Their values are listed in Table 1.

As expected, the electrolyte resistance (R_e) was found to be quite stable as it depends only on the supporting electrolyte concentration (0.5 M NaCl). The charge transfer resistance (R_{ct}) was also nearly unchanged as its value depends on the redox tracer, which was the same throughout the experiments, and also is not influenced by convection at the equilibrium potential. The CPE elements, Q_{dl} and n, can be converted into an equivalent frequency-independent capacitance C_{eq} calculated according to the formula of Brug et al. [31] as:.

$C_{eq} = Q^{1/n} R e^{\frac{1-n}{n}}$ in which R_{ct} was ignored since.$R_{ct}^{-1} \ll R_e^{-1}$

The C_{eq} values reported in Table 1 display only slight variations with the flow rate (7.53 ± 0.28 μF.cm^{-2}).

The R_{ct} values can also be converted to give an estimate of the heterogeneous charge transfer rate constant k_0 as follows:.

$k_0 = RT/F^2 SR_{ct,\eta\to 0}[C]$ in which T is the temperature (298.16 K), R the molar gas constant (8.31446 J.mol^{-1}.K^{-1}), F the Faraday constant (96485.3C.mol^{-1}), S the surface area of the WE microelectrode (9.10^{-5} cm^2), and $R_{ct,\eta\to 0}$ the charge transfer resistance (~1 MΩ or 100 Ω.cm^2) at zero overpotential. The k_0 values reported in Table 1 (~10^{-3}cm.s^{-1}) are in the expected range for the $Fe(CN)_6^{4-}/Fe(CN)_6^{3-}$ system.

Considering the dependence of the properties of the convective–diffusion impedance on the flow rate, one can firstly observe the increase in the characteristic frequency with the flow rate: in Fig. 3, two EIS plots performed on the same chip with a flow rate equal to 0.01 μL s^{-1} (panel A), and 0.1 μL s^{-1} (panel B) are compared. A net change in the EIS shape is observed: the second loop, characteristic of the convective–diffusion impedance in the lower frequency domain, is shifted to higher frequencies for the highest value of the volumetric flow and then becomes merged with the loop due to the parallel arrangement R_{ct}//CPE(Q,n). Secondly, the convective–diffusion resistance R_D decreases with the flow rate from 0.01 to 0.2 μL s^{-1}. This is in qualitative agreement with an increase in the current, as expected in channel microelectrode hydrodynamics [6].

More quantitatively, the R_D dependence on the flow rate can be deduced from reference [16] where Z_D, proportional to the measured convective–diffusion impedance, was expressed for a thin rectangular electrode across the flow direction as:.

$Z_D^{-1} = -\int_0^d dz \int_0^{x_e} \frac{\partial h}{\partial \eta}\Big|_0 \frac{dx}{\delta(x)}$ and then $Z_D^{-1}(0) = R_D^{-1} = -d\left(\frac{\alpha x_e^2}{D}\right)^{\frac{1}{3}} DH(\sigma)$ for σ → 0.

Equation (16) in reference [16] gives the expression of $H(\sigma')$ which has a constant limit of $-\frac{3}{2}\frac{dh_0}{d\eta}$ when σ → 0. The product $R_D \times \left(\frac{\alpha x_e^2}{D}\right)^{\frac{1}{3}}$ should then be constant. This appears to be a reasonable approximation when this quantity is plotted as function of $\left(\frac{\alpha x_e^2}{D}\right)^{\frac{1}{3}}$ (see Fig. 3C).

One can also observe that the limiting diffusion current, I_{lim}, proposed by L.P. Reiss and T.J. Hanratty [32] in the case of a thin rectangular electrode (d and x_e in Fig. 1C,D) is proportional to the quantity $dD\left(\frac{\alpha x_e^2}{D}\right)^{\frac{1}{3}}$. Therefore R_D is accordingly found to be inversely proportional to the limiting diffusion current, though measured here at the rest potential. This also validates the use of equations (1)–(7) for the present experimental conditions, corresponding to convective diffusion [33,34].

The quantity $\frac{\alpha x_e^2}{D}$ was earlier proposed by Ling in [35] as a criterion for pure established convective diffusion conditions for the same electrode geometry (i.e. ignoring the diffusive term in the x direction). He postulated that one should impose $\frac{\alpha x_e^2}{D} \geq 5000$. However, for the lowest flow rate, which corresponds here to $\frac{\alpha x_e^2}{D} \approx 10^2$, convective diffusion conditions are already valid, as shown by the EIS data.

This confirms that, for flow rates in the range from 0.01 to 0.2 μL s^{-1}, natural diffusion can be disregarded in comparison to convective diffusion.

4. Conclusions

In this work, electrochemical impedance spectroscopy (EIS) data were obtained for a rapid redox system on a microband electrode placed crosswise in a rectangular microfluidic channel under Poiseuille flow. The results were analyzed by use of a Randles equivalent circuit where special attention was focused on the diffusion–convection impedance. It was shown that a quantitative analytical expression for this impedance established earlier for a thin microband electrode is in perfect agreement with the experimental impedance and therefore validates the use of this expression for a microfluidic channel. It can be inferred that this conclusion is consistent with the fact that in the present geometry the diffusion layer can develop without being constrained by the opposite wall.

It can also be concluded that in more complicated systems, where the Randles equivalent circuit involves intricate elements, accurate determination of these elements would require such a quantitative expression for the convective–diffusion impedance, especially if it is the dominant term.

5. Data availability

The data that support the findings of this study are available from the corresponding authors upon reasonable request.

CRediT authorship contribution statement

Claire Poujouly: Conceptualization, Methodology, Investigation, Resources, Formal analysis, Visualization, Validation. **Pedro Gonzalez-Losada:** Conceptualization, Methodology, Investigation, Resources, Formal analysis. **Rassen Boukraa:** Investigation, Formal analysis. **Martina Freisa:** Methodology, Resources, Formal analysis. **Jérémy Le Gall:** Methodology, Resources, Formal analysis. **David Bouville:** Methodology, Investigation, Resources. **Claude Deslouis:**

Table 1
Modified Randles circuit parameters used for fitting with equations (1–7) in all Figures.

F_V μL.s^{-1}	F_V cm^3.s^{-1}	$(F_V)^{1/3}$ cm. s$^{-1/3}$	α s^{-1}	$(\alpha x_e^2/D)^{1/3}$	R_D Ω.cm^2	R_e Ω	R_{ct} Ω.cm^2	10^3 k_0 cm.s^{-1}	10^9 Q_{dl} Ω^{-1}s^n	n	C_{eq} μF. cm^{-2}	X(*)%
0.01	1 10^{-5}	0.0215	80	4.160	23.23	1458.1	81.17	1.093	3.087	0.889	7.37	0.925
0.05	5 10^{-5}	0.0368	400	7.114	17.031	1458.9	82.49	1.076	3.127	0.888	7.37	0.98
0.08	8 10^{-5}	0.0431	640	8.320	10.503	1449.6	70.73	1.25	3.694	0.876	7.37	1.02
0.1	1 10^{-4}	0.0464	800	8.963	7.19	1446.7	101.07	0.88	3.905	0.875	7.72	1.10
0.2	2 10^{-4}	0.0585	1600	11.292	4.56	1449.5	100.77	0.88	4.286	0.869	7.81	1.14

(*) Values of the resulting χ^2 statistic were obtained with errors of fitted values, σ = 0.01, for frequencies ranging from 1 MHz to 0.1 Hz.

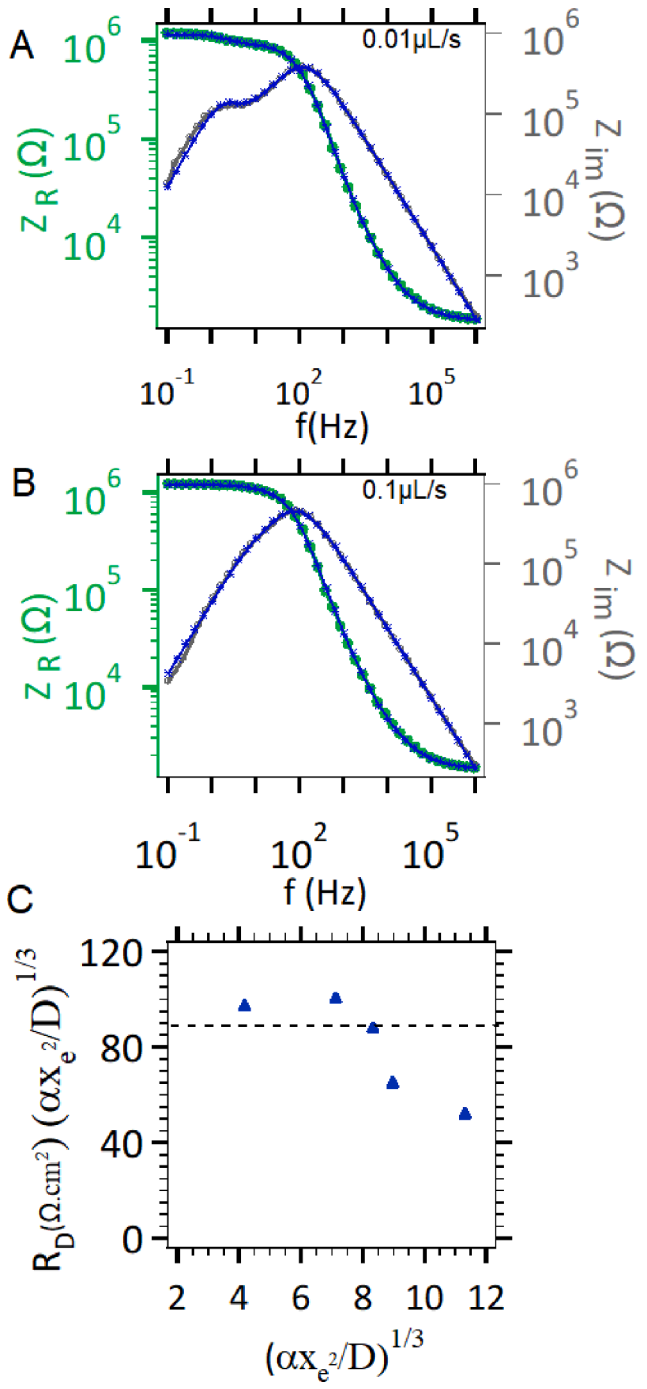

Fig. 3. EIS Bode plots for experimental and modeled impedances from 1 MHz to 0.1 Hz with 10 mV AC signal excitation, for different volumetric flow rates (**A**) 0.01 µL s^{-1}. (**B**) 0.1 µL s^{-1}. (**C**) Variation of $R_D \times \left(\frac{\alpha x_e^2}{D}\right)^{\frac{1}{3}}$ with $\left(\frac{\alpha x_e^2}{D}\right)^{\frac{1}{3}}$ in the range of volumetric flow lower from 0.01 to 0.2 µL s^{-1}. See Table 1 and equations (1–7).

Conceptualization, Formal analysis, Software, Visualization, Validation. **Jean Gamby:** Conceptualization, Methodology, Investigation, Formal analysis, Software, Supervision, Visualization, Validation, Resources, Project administration, Funding acquisition, Writing- Original draft, Review and Editing.

Declaration of Competing Interest

The authors declare that they have no known competing financial interests or personal relationships that could have appeared to influence the work reported in this paper.

Acknowledgements

The authors would like to thank the DIMELEC project ANR-19-CE09-0016 for funding and RENATECH clean room facilities at C2N, Palaiseau, France. C.P. thanks the doctoral school “Electrical, Optical, Bio-Physics and Engineering” (ED575) and Paris-Saclay University for PhD grants.

References

[1] R.G. Compton, A.C. Fisher, R.G. Wellington, P.J. Dobson, P.A. Leigh, Hydrodynamic voltammetry with microelectrodes: channel microband electrodes; theory and experiment, J. Phys. Chem. 97 (1993) 10410–10415.
[2] C. Amatore, C. Sella, L. Thouin, Electrochemical time-of-flight responses at double-band generator-collector devices under pulsed conditions, J. Electroanal. Chem. 593 (1-2) (2006) 194–202.
[3] M. Faure, A. Pallandre, S. Chebil, I. Le Potier, M. Taverna, B. Tribollet, C. Deslouis, A.-M. Haghiri-Gosnet, J. Gamby, Improved electrochemical detection of a transthyretin synthetic peptide in the nanomolar range with a two-electrode system integrated in a glass/PDMS microchip, Lab Chip 14 (15) (2014) 2800–2805.
[4] M.S. Chiriacò, E. Primiceri, E. D'Amone, R.E. Ionescu, R. Rinaldi, G. Maruccio, EIS microfluidic chips for flow immunoassay and ultrasensitive cholera toxin detection, Lab Chip 11 (4) (2011) 658–663.
[5] K. Aoki, K. Tokuda, H. Matsuda, Hydrodynamic voltammetry at channel electrodes: Part VIII. Theory of reversible voltammograms for chronoamperometry and linear sweep voltammetry, J. Electroanal. Chem. Interfacial Electrochem. 209 (2) (1986) 247–258.
[6] R.G. Compton, C.E. Banks, Hydrodynamic Electrodes, in: Understanding Voltammetry, Imperial College Press, 2010, pp. 291–346.
[7] C. Amatore, N. Da Mota, C. Sella, L. Thouin, Theory and experiments of transport at channel microband electrodes under laminar flow. 3. Electrochemical detection at electrode arrays under steady state, Anal. Chem. 82 (6) (2010) 2434–2440.
[8] M.C. Horny, M. Lazerges, J.M. Siaugue, A. Pallandre, D. Rose, F. Bedioui, C. Deslouis, A.M. Haghiri-Gosnet, J. Gamby, Electrochemical DNA biosensors based on long-range electron transfer: investigating the efficiency of a fluidic channel microelectrode compared to an ultramicroelectrode in a two-electrode setup, Lab Chip 16 (2016) 4373–4381.
[9] T.M. Squires, R.J. Messinger, S.R. Manalis, Making it stick: convection, reaction and diffusion in surface-based biosensors, Nat. Biotechnol. 26 (2008) 417–426.
[10] J.E.B. Randles, Kinetics of rapid electrode reactions, Discuss. Faraday Soc. 1 (1947) 11–19.
[11] M. Fleischmann, S. Pons, J. Daschbach, The AC impedance of spherical, cylindrical, disk, and ring microelectrodes, J. Electroanal. Chem. Interfacial Electrochem. 317 (1-2) (1991) 1–26.
[12] P. Tamiasso-Martinhon, H. Cachet, C. Deslouis, V. Vivier, Amorphous carbon nitride a-CNx microelectrode: fabrication and characterization, Electrochem. Commun. 12 (2010) 1074–1076.
[13] R.G. Compton, G.R. Sealy, The theory of the AC voltammetry of reversible electrode processes at tubular electrodes, J. Electroanal. Chem. Interfacial Electrochem. 145 (1) (1983) 35–41.
[14] R.G. Compton, M.E. Laing, P.R. Unwin, AC impedance measurements at channel electrodes: the effect of convection, J. Electroanal. Chem. Interfacial Electrochem. 207 (1-2) (1986) 309–314.
[15] C. Deslouis, B. Tribollet, M.A. Vorotyntsev, Diffusion-convection impedance at small electrodes, J. Electrochem. Soc. 138 (9) (1991) 2651–2657.
[16] C. Deslouis, O. Gil, B. Tribollet, Frequency response of small electrodes to hydrodynamic or to potential perturbations, Electrochim. Acta 38 (14) (1993) 1847–1856.
[17] R.G. Compton, J. Winkler, Hydrodynamic voltammetry with channel microband electrodes: alternating current impedance measurements, J. Phys. Chem. 99 (1995) 5029–5034.
[18] M.-C. Horny, F. Billon, C. Deslouis, M. Lazerges, V. Dupuis, J.-M. Siaugue, A. Pailleret, J. Gamby, Amorphous carbon nitride microband integrated in a microfluidic device for DNA biosensors applications, J. Electroanal. Chem. 895 (2021), 115395.
[19] T. Holm, M. Ingdal, E.V. Fanavoll, S. Sunde, F. Seland, D.A. Harrington, Mass-transport impedance at channel electrodes: accurate and approximate solutions, Electrochim. Acta 202 (2016) 84–89.
[20] H. Jung Lee, S.-J. Bai, Y. Seok Song, Microfluidic electrochemical impedance spectroscopy of carbon composite nanofluids, Sci. Rep. 7 (2017) 722.
[21] K. Krukiewicz, Electrochemical impedance spectroscopy as a versatile tool for the characterization of neural tissue: a mini review, Electrochem. Commun. 116 (2020) 106742.

[22] T. Holm, M. Ingdal, J.R. Strobl, E.V. Fanavoll, S. Sunde, F. Seland, D.A. Harrington, Generator-sensor impedance at double channel electrodes, Electrochim. Acta 229 (2017) 452–457.
[23] M.-C. Horny, V. Dupuis, J.-M. Siaugue, J. Gamby, Release and detection of microRNA by combining magnetic hyperthermia and electrochemistry modules on a microfluidic chip, Sensors 21 (2021) 185.
[24] L.M. Peter, W. Dürr, P. Bindra, H. Gerischer, The influence of alkali metal cations on the rate of the Fe(CN)64−/Fe(CN)63− electrode process, J. Electroanal. Chem. Interfacial Electrochem. 71 (1) (1976) 31–50.
[25] J.A. Alden, R.G. Compton, Microband electrodes of ideal and nonideal geometries: AC impedance spectroscopy, Electroanalysis 8 (1996) 30–33.
[26] G. Ferreira, A. Sucena, L.L. Ferrás, F.T. Pinho, A.M. Afonso, Hydrodynamic entrance length for laminar flow in microchannels with rectangular cross section, Fluids 6 (7) (2021) 240.
[27] B. Hirschorn, M.E. Orazem, B. Tribollet, V. Vivier, I. Frateur, M. Musiani, Constant-phase-element behavior caused by resistivity distributions in films: I. Theory, J. Electrochem. Society 157 (2010) C452–C457.
[28] M. Musiani, M.E. Orazem, N. Pébère, B. Tribollet, V. Vivier, Constant-phase-element behavior caused by coupled resistivity and permittivity distributions in films, J. Electrochem. Soc. 158 (2011) C424–C428.
[29] M. Faure, F. Billon, A.M. Haghiri-Gosnet, B. Tribollet, C. Deslouis, A. Pailleret, J. Gamby, Influence of the atomic nitrogen content in amorphous carbon nitride thin films on the modulation of their polarizable interfaces properties, Electrochim. Acta 280 (2018) 238–247.
[30] M.E. Orazem, N. Pébère, B. Tribollet, Enhanced graphical representation of electrochemical impedance data, J. Electrochem. Soc. 153 (2006) B129–B136.
[31] G.J. Brug, A.L.G. van den Eeden, M. Sluyters-Rehbach, J.H. Sluyters, The analysis of electrode impedances complicated by the presence of a constant phase element, J. Electroanal. Chem. Interfacial Electrochem. 176 (1-2) (1984) 275–295.
[32] L.P. Reiss, T.J. Hanratty, An experimental study of the unsteady nature of the viscous sublayer, AIChE J. 9 (2) (1963) 154–160.
[33] A.M. Lévêque, Les lois de la transmission de chaleur par convection, Ann. Mines 13 (1928) 283–287.
[34] V.G. Levich, Physicochemical Hydrodynamics, Prentice-Hall, 1962.
[35] S.C. Ling, Heat transfer from a small isothermal spanwise strip on an insulated boundary, J. Heat Transfer 85 (1963) 230–235.